Computer Modeling in Engineering & Sciences CMES, vol.122, no.3, pp.805-830, 2020

Numerical Analysis on Multi-Field Characteristics and Synergy in a Large-Size Annular Combustion Chamber with Double Swirlers

Zaiguo Fu[1, *], Huanhuan Gao[1], Zhuoxiong Zeng[1] and Jiang Liu[1]

Abstract: In order to comprehensively evaluate the flow and heat transfer performance of a large-size annular combustion chamber of a heavy-duty gas turbine, we carried out numerical computation and analyses on the velocity, temperature and pressure fields in the chamber with double swirlers. The mathematical model of the coupling combustion, gas flow, and heat transfer process was established. The influences of the inlet swirling strength, fuel-air ratio and temperature of the premixed gas on the multi-field characteristics and synergy were investigated on the basis of field synergy theory. The results showed that the central recirculation zone induced by the inlet swirling flow grows downstream in the combustion chamber. The velocity and temperature in the outlet section of the chamber tend to be uniform due to the upstream improved synergy. The outer swirl number of the premixed gas flow has a great influence on the comprehensive flow and heat transfer performance of the combustion chamber. The synergy angles change towards benefiting the synergy between velocity and temperature fields with the increasing swirl numbers and inlet gas temperature while the velocity-pressure synergy becomes poor. The increasing fuel-air ratio of premixed gas leads to different trends of the velocity-temperature synergy and velocity-pressure synergy. The comprehensive synergy representing the low-resistance heat transfer performance is evidently dominated mainly by the velocity-temperature synergy.

Keywords: Annular combustor, heat transfer, multi-field synergy, synergy angle, swirling flow.

1 Introduction

The gas turbine generator set has strong maneuverability and can be started rapidly without external power. It has been widely used in the power generation industry to meet the peak load demand and ensure the safe operation of the power grid [Lee, Kim and Kim (2017); Ayodele, Vincent, Claudius et al. (2019)]. The heavy-duty gas turbine is an important component of the gas turbine generator set. The output of the gas turbine is greatly dominated by the performance of the combustion chamber. Accordingly, it is

[1] College of Energy and Mechanical Engineering, Shanghai University of Electric Power, Shanghai, 200090, China.
[*] Corresponding Author: Zaiguo Fu. Email: fuzaiguo2009@hotmail.com.
Received: 14 October 2019; Accepted: 19 November 2019.

necessary to investigate the combustion process coupled with the gas flow and heat transfer in the chamber to find ways to ensure the reliable operation of gas turbine.

At present, the method to generate a recirculation zone in the combustion chamber is employed widely for making a stable combustion. In general, the inlet gas rotates under the action of swirler set on the head of combustor and a low-pressure zone is formed in the center when the rotary gas flow is with a certain swirling strength. The ignited high-temperature gas flows back due to the adverse pressure gradient, inducing a strong heat and mass exchange between the main flow and the backflow. The entered mixed gas is heated and ignited continuously [Li, Jiang, Zhu et al. (2019)].

Therefore, a stable combustion generated in the combustion chamber is greatly affected by the swirling strength of the inlet gas flow. Anacleto et al. [Anacleto, Fernandes, Heitor et al. (2003)] studied the swirling flow in a lean premixed prevaporized combustor using high-speed photography technique. The results showed that the central recirculation zone appeared when the swirl number was greater than 0.5. Tsao et al. [Tsao, He, Wang et al. (1999)] numerically investigated the inlet radial swirling gas flow and the swirling level in the inlet section of the combustion chamber by using the Reynolds stress transport model (RSTM). The results showed that the strength of the centerline vortex core depended on the vortex level of inlet swirling flow and the swirling flow caused a strong streamlined pressure change and a change in the structure of the recirculation zone. In addition, the results also showed that the RSTM could reproduce the flow in the chamber and reflect the effect of the inlet vortex level on the internal flow structure. Some other researchers have focused on the flow structures of the swirling flows caused by combined jets under different swirl numbers [Vishwanath, Tilak and Chaudhuri (2018); Palm, Grundmann, Weismüller et al. (2006)]. The results have shown that the velocity distribution varies with the inlet swirling strength.

Apart from this swirling strength, many other factors, such as the temperature and equivalence ratio of the inlet gas can also affect the flow field, heat transfer and combustion performance of the combustion chamber. Huang et al. [Huang and Yang (2004)] found that the inlet temperature and equivalence ratio are the two most important variables to determine the combustion stability in combustion chamber by investigating the transition of flame structure from stable to unstable state. The results indicated that the increase of inlet mixture temperature gave rise to the flame in the central recirculation zone penetrating to the angular recirculation zone and caused the sudden increase of acoustic flow oscillation. Chen et al. [Chen, Ruan, Yu et al. (2019)] studied the influence of inlet fuel type and temperature on the combustion stability. The results showed that the flame in combustion chamber was stable when linear alkane was used as fuel. A unique mode-shift phenomenon arose in the combustion chamber when the inlet air temperature increased from 403 K to 423 K. Han et al. [Han, Laera, Morgans et al. (2019)] also studied the influence of inlet temperature on the combustion instability for a certain combustion chamber. They reported that the high inlet temperature promoted the evaporation of fuel in the combustion chamber to some extent and the combustion instability suddenly reduced when the inlet temperature exceeded 570 K. Moreover, some researchers investigated the effect of equivalence ratio of fuel on combustion instability, flame temperature, state switching and combustion products in the combustor [Worth and

Dawson (2017); Aklouche, Loubar, Bentebbiche et al. (2017)]. All the results proved that the factor of equivalence ratio has significant influences on the combustion performance of the combustor.

The overall performance of the chamber is greatly related to the synergy among the velocity field, temperature field and pressure field due to the coupling effect among the flow, heat transfer and combustion process in the combustion chamber. According to the field synergy theory proposed by Guo et al. [Guo, Li and Wang (1998); Guo, Tao and Shah (2005)], the better synergy degree among the three fields is, the stronger heat transfer effect and lower flow resistance will be obtained. This field synergy principle has been widely applied to evaluating the overall performance of the heat exchange equipments in some research fields.

Tao et al. [Tao, Guo and Wang (2002); Tao, He, Wang et al. (2002)] analyzed the characteristics and mechanism of the enhanced single phase convective heat transfer based on the field synergy principle. This principle was verified as a guide for the design of heat exchange equipment. To further develop this principle, He et al. [He, Lei, Tian et al. (2009)] and Liu et al. [Liu, Liu and Huang (2010); Liu, Liu, Wang et al. (2018)] conducted analyses of three-field synergy on heat transfer augmentation with low pressure drop for the laminar and turbulent convective flow. The synergy among the velocity field, temperature field and pressure field was thought to be important for heat transfer enhancement with low penalty of pressure drop. Xie et al. [Xie, He, Zhang et al. (2018)] conducted a numerical simulation of a closed wet cooling tower equipped with longitudinal finned tubes. The synergy among velocity, temperature and humidity was applied to analyzing the effects of coolant velocity, number and height of fins on the distribution of vortex.

Recently, Liu et al. [Liu, Liu, Dong et al. (2019)] discussed the constitutive relationship between fluid dynamic flux and pressure gradient aiming to ascertain the physical characteristics of enhanced convective heat and mass transfer. This work firstly revealed the multi-field synergy among velocity, pressure, temperature and component concentration in the convective heat and mass transfer phenomena. It provided an extended synergy principle to evaluate the heat and mass transfer performance. Zeng et al. [Zeng, Wang, Tian et al. (2015)] conducted a multi-field synergy analysis on an advanced vortex combustor by numerical simulation. The results indicated that increasing the inlet velocity and decreasing the inlet temperature could raise the overall performance of heat transfer enhancement. It is worth mentioning that in their work, the vortex combustor used trapped vortex combustion technology. It differs from the swirling combustion adopted in the large-size annular combustion chamber. At present, it has not been seen the special publication of literature on the application of field synergy theory in the annular combustor with swirling combustion.

Against this background, we propose a numerical analysis on the multi-field characteristics and synergy in a large-size annular combustion chamber to find appropriate inlet parameters to improve the overall performance of the chamber for a heavy-duty gas turbine. The combustion chamber employs double-swirler inlets. The swirling strength, temperature and equivalence ratio of the inlet premixed gas flow are taken into consideration. The influences of these factors on the velocity field, temperature

field, pressure field and their synergy are discussed by means of the analyses on the variations of velocity and temperature distributions and three field synergy angles.

2 Numerical modeling and solution

2.1 Physical model and discrete grids

The research object is a three-dimensional (3D) annular combustor of a heavy-duty gas turbine. There are altogether 24 double-swirler inlets which are distributed uniformly over the entire arc head. The present study takes 1/24 of the combustion chamber as the target. The schematic diagram of the center section is shown in Fig. 1(a) to demonstrate the double-swirler inlet. The premixed gas enters the combustion chamber and becomes a swirling flow under the function of swirlers.

In order to simplify the simulation and accelerate the convergence of the calculation, we adopt the following assumptions: (1) the blade structure of swirler is ignored and each inlet is simplified as a double-swirler inlet with an inner round hole and a concentric annular hole; (2) the micro mixing holes on the combustor wall are ignored. It is assumed that they have no significant influence on combustion and flow in the main combustion section according to the introduction in literature [Mohammad, Jeng and Andac (2010); Tsao and Lin (1999)]. The diameter of the inlet inner hole is 0.084 m ($2R$, R=0.042 m). The annular hole is $1.5R$ wide. The total length of the combustor is $30.8R$. The height of the annular outlet is $3.4R$. Other geometric parameters are shown in the schematic diagram of the center section of the computational domain as the Fig. 1(b).

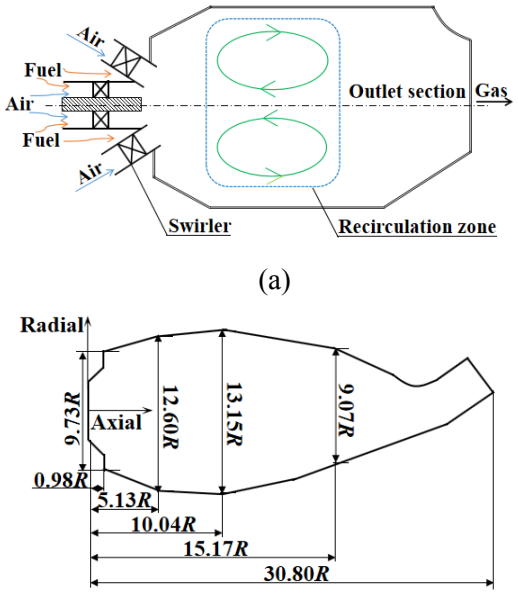

Figure 1: Schematic diagram of center section of (a) 1/24 annular combustor and (b) computational domain

Additionally, four characteristic lines are selected for quantitative analysis of the calculated results on velocity and temperature. The characteristic lines are all perpendicular to the central axis, and the distances from them to the entrance of combustion chamber are 0.98*R*, 5.13*R*, 10.04*R*, and 15.17*R* respectively. They are shown in Fig. 1(b) with the local coordinate. The axial direction is defined as *x*. Thus, the positions of the four lines are located at *x*=0.98*R*, 5.13*R*, 10.04*R*, 15.17*R*, respectively. The outlet section of the combustor chamber is from *x*=10.04*R*. The rest is defined as the inlet section.

The code of ICEM CFD 15.0 software is employed for meshing the computational domain. The grids of the swirling inlet are locally refined due to its relatively small size. The grids near the combustor wall are also refined so as to accurately capture the abrupt changes of physical parameters. The unstructured grids of the computational domain are shown in Fig. 2.

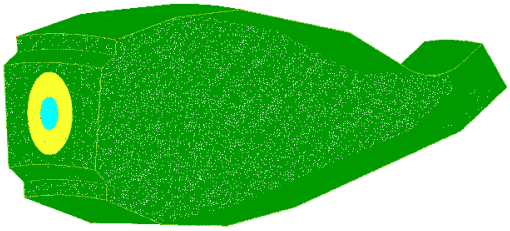

Figure 2: Grids of computational domain

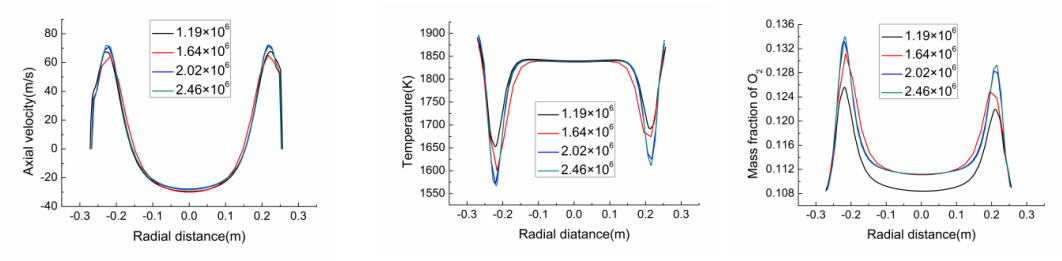

(a) (b) (c)

Figure 3: Results of (a) axial velocity, (b) temperature and (c) mass fraction of O_2 on the characteristic line at *x*=5.13*R* under various grid numbers

In this study, four sets of grids with the number of 1.19 million, 1.64 million, 2.02 million and 2.46 million are adopted to conduct the grid independence validation. The results of the reacting flow in the combustor under the same working condition are compared. Figs. 3(a)-3(c) show the axial velocity, temperature and mass fraction of O_2 at different radial positions on the characteristic line at *x*=5.13*R*, respectively. It can be seen from Fig. 3 that the predicted results of flow field, heat transfer and species transfer by using 2.02 million grids are very close to those by using 2.46 million grids. The maximum deviation is 1.17% for the mass fraction of O_2 on the characteristic line. Thus, the number of 2.02 million is set to be the grids number for the numerical computation in present study.

2.2 Mathematic model

2.2.1 Governing equations

In the combustion process, the turbulent flow, heat and mass transfer can be described by the general mass, momentum, energy and composition conservation equations [Nam, Lee, Joo et al. (2019)].

The realizable k-ε model is adopted since it adds rotation and curvature related terms to the turbulent viscosity calculation formula. It can solve the uniform shear flow of rotation and problems effectively [Karim and Bart (2006); Zhang, Zheng and Zhao (2013); Jin, Zhang and Gu (2008)]. The turbulent kinetic energy k of the realizable k-ε model and its dissipation rate ε are expressed as follows:

$$\rho\frac{dk}{dt}=\frac{\partial}{\partial x_i}\left[(\mu+\frac{\mu_t}{\sigma_k})\frac{\partial k}{\partial x_i}\right]+G_k+G_b-\rho\varepsilon-Y_M \tag{1}$$

$$\rho\frac{d\varepsilon}{dt}=\frac{\partial}{\partial x_i}\left[\left(\mu+\frac{\mu_t}{\sigma_\varepsilon}\right)\frac{\partial\varepsilon}{\partial x_i}\right]+\rho C_1 S\varepsilon-\rho C_2\frac{\varepsilon^2}{k+\sqrt{\nu\varepsilon}}+C_{1\varepsilon}\frac{\varepsilon}{k}C_{3\varepsilon}G_b \tag{2}$$

In Eqs. (1) and (2), G_k represents the generation of turbulent kinetic energy caused by the average velocity gradient. G_b represents the generation of turbulent kinetic energy due to the influence of buoyancy. Y_M represents the effect of compressible turbulent pulsation expansion on the total dissipation rate. C_1, C_2, $C_{1\varepsilon}$ and $C_{3\varepsilon}$ are constants. σ_k and σ_ε are the turbulent Prandtl constants of turbulent kinetic energy and its dissipation rate. S is the swirl number. μ_t is the turbulent viscosity. β is the coefficient of thermal expansion. g_i is turbulent viscosity reduction term. C_μ is a function of the average strain rate and swirl number.

Based on the two-step global reaction of methane, it is considered that the fuel of pure methane and air are completely premixed when they reach the inlet. The premixed combustion occurs in the annular combustion chamber. The finite rate/vortex dissipation turbulent combustion model is adopted for combustion. The reaction rate and eddy dissipation rate are calculated as follows:

$$W=kC_A^aC_B^b=k_0\exp(-\frac{E}{RT})C_A^aC_B^b \tag{3}$$

$$R_{i,r}=v_{i,r}^{'}M_{w,i}AB\rho\frac{\varepsilon}{k}\frac{\sum_p Y_p}{\sum_j^N v_{j,r}^{''}M_{w,j}} \tag{4}$$

In Eqs. (3) and (4), ε/k controls the reaction rate. k_0 is the pre-factor. E is the activation energy. C is the reactant concentration. R is the gas constant. T is the temperature. Y_p is the mass fraction of the product. $M_{w,i}$, $M_{w,j}$ are the molecular weights of the substances i and j, respectively. ρ is the density. $v'_{i,r}$ is the stoichiometric number of the reactant i in the reaction r. $v''_{j,r}$ is the stoichiometric number of the product j in the reaction r. In Eq. (3), C_A and C_B are the concentrations of reactants A and B, respectively. a and b are chemical reaction coefficients. In Eq. (4), A and B are empirical constants as 4.0 and 0.5, respectively.

The reaction mechanism of methane and air is expressed as follows [E, Liu, Zhao et al. (2018)].

$$2CH_4+3O_2=2CO+4H_2O \tag{5}$$

$$2CO+O_2=2CO_2 \tag{6}$$

2.2.2 Field synergy angles

The field synergy principle confirms that the convective heat transfer intensity is not only related to the velocity, temperature difference and physical properties of the fluid, but also closely related to the coordination of velocity and heat flux. The field synergy principle is developed by using more than one synergy angle (i.e., the included angle between different vectors) to describe the multi-field synergy aiming to ascertain the flow resistance, heat transfer and the comprehensive performance. The synergy angle β between velocity and temperature gradient, the synergy angle θ between velocity and pressure gradient, the synergy angle γ between temperature gradient and velocity gradient [Liu, Liu, Wang et al. (2018); Tang, Chu, Ahmed et al. (2016); Lu and Zhou (2016); Zhang, Wang, Zhu et al. (2015)] are given as Eqs. (7)-(9) respectively. According to the field synergy principle, the smaller β and θ, and the larger γ indicate better synergies.

$$\beta = \arccos\frac{|U\cdot\nabla T|}{|U||\nabla T|} = (\frac{180}{\pi})\arccos\left|\frac{u\frac{\partial T}{\partial x}+v\frac{\partial T}{\partial y}+w\frac{\partial T}{\partial z}}{\sqrt{u^2+v^2+w^2}\sqrt{(\frac{\partial T}{\partial x})^2+(\frac{\partial T}{\partial y})^2+(\frac{\partial T}{\partial z})^2}}\right| \tag{7}$$

$$\theta = \arccos\frac{|U\cdot\nabla P|}{|U||\nabla P|} = (\frac{180}{\pi})\arccos\left|\frac{u\frac{\partial p}{\partial x}+v\frac{\partial p}{\partial y}+w\frac{\partial p}{\partial z}}{\sqrt{u^2+v^2+w^2}\sqrt{(\frac{\partial p}{\partial x})^2+(\frac{\partial p}{\partial y})^2+(\frac{\partial p}{\partial z})^2}}\right| \tag{8}$$

$$\gamma=\arccos\frac{|\nabla T\cdot\nabla U|}{|\nabla T||\nabla U|} = (\frac{180}{\pi})\arccos\left|\frac{\frac{\partial T}{\partial x}\frac{\partial u}{\partial x}+\frac{\partial T}{\partial y}\frac{\partial u}{\partial y}+\frac{\partial T}{\partial z}\frac{\partial u}{\partial z}}{\sqrt{(\frac{\partial T}{\partial x})^2+(\frac{\partial T}{\partial y})^2+(\frac{\partial T}{\partial z})^2}\sqrt{(\frac{\partial u}{\partial x})^2+(\frac{\partial u}{\partial y})^2+(\frac{\partial u}{\partial z})^2}}\right| \tag{9}$$

The volumetric average synergy angle is defined as Eq. (10).

$$\theta_{\mathrm{m}} = \frac{\sum\theta_i \mathrm{d}V_i}{\sum \mathrm{d}V_i} \tag{10}$$

In the above equation, θ_i is the synergy angle in the ith element. $\mathrm{d}V_i$ is the ith element of control volume.

2.2.3 Boundary conditions

A local cylindrical coordinate system is applied to setting the velocity components for the inlet swirling flow. The swirl number defined as the ratio of the rotational moment of momentum to axial moment of momentum is set as 0.8. According to the practical settings for the inlet [Gao, Fu, Zeng et al. (2019)], the swirl number is expressed as:

$$S = \frac{2W}{3U} \tag{11}$$

In Eq. (11), W stands for the tangential velocity. U stands for the axial velocity. The outlet is set as the pressure outlet and the pressure is 1823900 Pa. The combustor wall is adiabatic. The side walls of the computational domain are periodic boundaries.

The adopted fuel is pure methane (CH_4). The main governing parameters under the designed working condition of the combustion chamber are as follows. The temperature of the inlet premixed gas is 697.24 K. The premixed gas enters the combustor at the equivalence ratio of 0.35 and 0.53 from the inner round hole and the outer annular hole, respectively. The corresponding fuel-air ratios are 2:98 and 3:97, respectively. The mass flow rates are 1.86 kg/s and 19.98 kg/s, respectively.

Table 1: Conditional parameters

Influence factor	Value
Inner swirl number	0.4, 0.6, 0.8, 1.0, 1.2
Outer swirl number	0.4, 0.6, 0.8, 1.0, 1.2
Fuel-air ratio	2:98, 3:97, 4:96, 5:95, 6:94
Inlet gas temperature (in K)	697.24, 600, 500, 400, 300

The values of the four influence factors including the inner swirl number of the flow from the inner hole, the outer swirl number of the flow from the outer annular hole, the fuel-air ratio, and the inlet gas temperature are listed in Tab. 1. The equivalence ratios corresponding to the fuel-air ratios of 4:96, 5:95 and 6:94 are 0.72, 0.91 and 1.10 respectively. The given values for a certain factor are adopted to investigate its influences on the multi-field synergy with other factors fixed as the designed values.

2.3 Numerical method and validation

The commercial ANSYS Fluent software was used in the calculation. The solution was based on the SIMPLE algorithm. The convection term was discretized by second-order upwind scheme and the diffusion term was discretized by second-order central difference scheme.

The validation of the present code was performed by a comparison between the obtained numerical results and the measured results from available literature as Orbay et al. [Orbay, Nogenmyr, Klingmann et al. (2013)]. In their study, the flow velocity in the central recirculation zone of a cylinder combustion chamber with an annular swirler was measured by PIV and LDV techniques. The inlet gas temperature was 670 K and the fuel-air ratio of the premixed gas was near 3:97. The inlet axial velocity was 30 m/s and the swirl number was 1.4. Thus, we present the normalized axial velocity in the core central recirculation zone accordingly. Its distribution along the radial direction from the center position to the chamber wall is shown in Fig. 4 with the measured results. The abscissas and ordinate represent the non-dimensional distance and axial velocity, respectively. As seen from Fig. 4, results obtained show good agreement with literature. Moreover, a similar experimental research on the temperature distribution in a simulated tested annular chamber was conducted by Dang [Dang (2009)]. The inlet gas temperature was 500 K, the fuel-air ratio was 0.03308 (i.e., 3.2:96.8) and the flow rate was 0.24 kg/s. As a

result, the temperature in the center section perpendicular to the chamber axis at the exit was uniform and the average value was 1673 K. In the present study, the calculated temperature is also uniform and the average value under the same condition is 1720 K. The deviation is in 2.8%. It is evident that the present model and method are valid for further calculations.

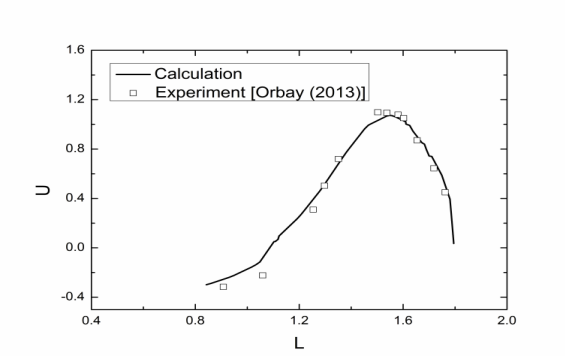

Figure 4: Comparison of axial velocity in the central recirculation zone between calculation and experimental results

3 Results and discussion

3.1 Baseline results

The calculated velocity field, temperature field, pressure field and their synergy function under the designed full-load condition of the gas turbine are taken as the baseline results. Fig. 5 shows the streamlines, isothermals and isopiestic lines in the center section of the combustion chamber.

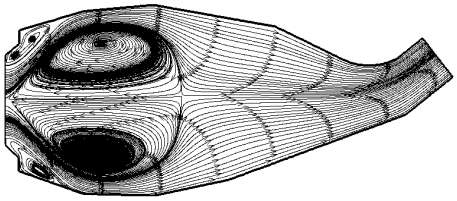

(a) Streamlines

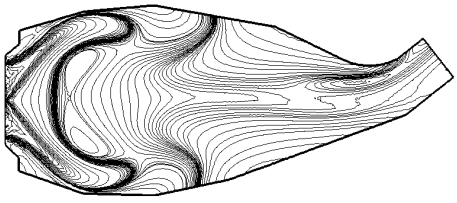

(b) Isothermals

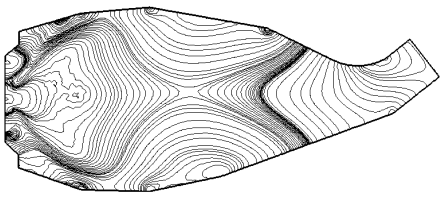

(c) Isopiestic lines

Figure 5: Baseline results of (a) streamlines, (b) isothermals and (c) isopiestic lines in the center section of combustion chamber

It can be seen from Fig. 5(a) that two large paired vortices appear in the inlet center section till the third boss at x=10.04R. The region dominated by the vortices is defined as the central recirculation zone. In this peach-shaped zone, most of the velocity vector is along the axial direction. Meanwhile, around the shoulder of the first boss at x=0.98R, two small vortices are generated along the upper and lower walls. This vortex region is defined as the corner recirculation zone.

From Fig. 5(b), it is observed that most of the isothermals in this central recirculation zone are along the radial direction and the temperature gradient is along the axial direction. Thus, the included angle between the velocity and temperature gradient is small, which will be introduced later as the synergy angle β.

From Fig. 5(c), it can be seen that in the central recirculation zone, most of the isopiestic lines are generally along the radial direction. Thus, the pressure gradient is in quasi-axial direction. This leads to a small included angle between velocity and pressure gradient, which will be introduced later as the synergy angle θ.

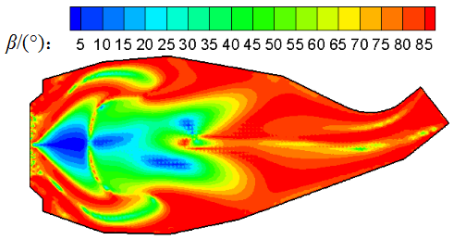

(a) β

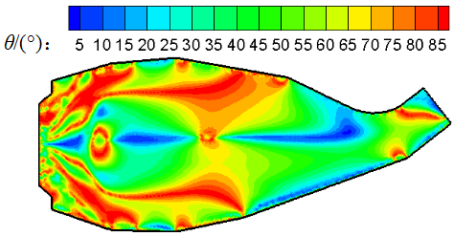

(b) θ

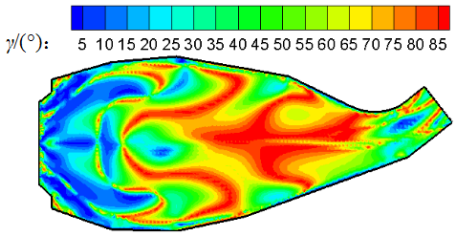

(c) γ

Figure 6: Baseline results of contours of (a) β, (b) θ and (c) γ in the center section of combustion chamber

Fig. 6 shows the contours of synergy angle β between velocity and temperature gradient, synergy angle θ between velocity and pressure gradient and synergy angle γ between velocity gradient and pressure gradient. The small synergy angle β in the central recirculation zone can be observed in Fig. 6(a). The average magnitude of synergy angle β in this zone is 37.7° according to the statistical calculation. According to the field synergy theory, the small synergy angle β signifies the excellent synergy between velocity and temperature gradient. It indicates that the heat transfer performance in the central recirculation zone is appropriate. However, out of this zone, the synergy angle β between velocity and temperature gradient is large, leading to a poor synergy and weak heat transfer.

From Fig. 6(b), the small synergy angle θ between velocity and pressure gradient in the central recirculation zone is observed. Thus, the excellent synergy between them can be speculated. Moreover, the small synergy angle θ is also observed in the outlet section from x=15.17R. The average magnitude of θ along the axis is 13.16° according to statistics. All of these indicate that the flow resistance generated in the central recirculation zone and in the outlet section is small under the designed working condition of the combustion chamber.

The synergy angle γ between velocity gradient and pressure gradient is small in the section from the inlet to the center of central recirculation zone as shown in Fig. 6(c). This small synergy angle indicates a poor overall performance of flow and heat transfer, which is thought to be caused by the undeveloped swirling flow with a large tangential velocity.

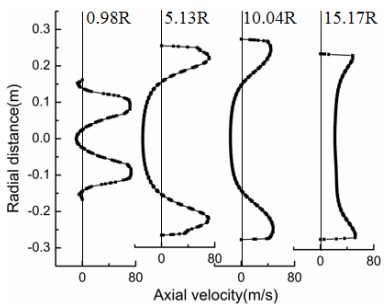

(a) Axial velocity

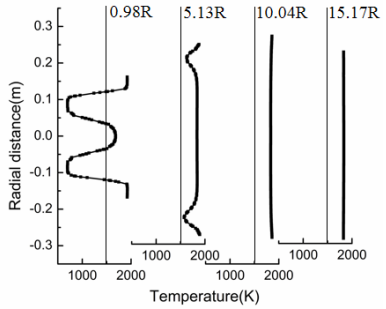

(b) Temperature

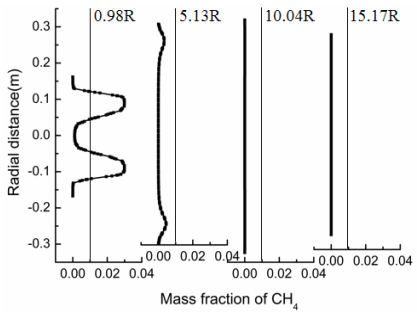

(c) Mass fraction of CH_4

Figure 7: Baseline results of (a) axial velocity, (b) temperature and (c) mass fraction of CH_4 on different characteristic lines at various axial locations

Moreover, the distribution of the axial velocity and temperature on different characteristic lines at various axial locations (x=0.98R, 5.13R, 10.04R and 15.17R) are presented in Fig. 7 as parts of baseline results to show the evolution of velocity and temperature under the field synergy function. From Fig. 7(a), it can be seen that the central negative axial velocity arises when the gas flow reaches at x=0.98R, corresponding to the first boss of the combustion chamber. The central negative velocity disappears at x=15.17R, corresponding to the fourth boss. This indicates that the central recirculation zone is located between the first boss and the fourth boss of the chamber. In addition, the axial velocity on the characteristic lines first increases and then decreases from the central axis to the chamber wall with the development of central recirculation zone. Around the shoulder of the first boss at x=0.98R, the corner recirculation zone with the negative axial velocity in near-wall region is formed.

As shown in Fig. 7(b), the near-wall temperature in the chamber is higher than that in the central recirculation zone caused by the heat accumulation in the corner recirculation zone at x=0.98R. However, in the outlet section from x=10.04R, the temperatures along the radial direction are uniform as 1839 K due to the excellent synergy function and heat transfer performance of the upstream central recirculation zone. From Fig. 7(c), it is found that a large amount of fuel is sucked into the corner recirculation zone as soon as it enters the combustion chamber due to the strong suction generated by the swirling flow. However, the fuel is exhausted in the outlet section after a rapid reaction in the upstream section.

3.2 Influence of swirl number

3.2.1 Inner swirl number

The axial velocity on the characteristic lines at x=0.98R and x=5.13R under various swirl numbers of the inlet flow from the inner hole (inner swirl numbers) are shown in Figs. 8(a) and 8(b) respectively.

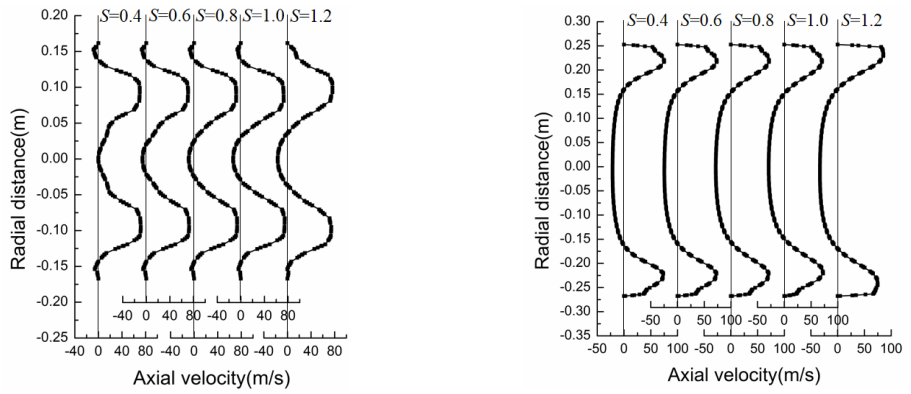

(a) x=0.98R (b) x=5.13R

Figure 8: Axial velocity on characteristic line at (a) x=0.98R and (b) x=5.13R under different inner swirl numbers

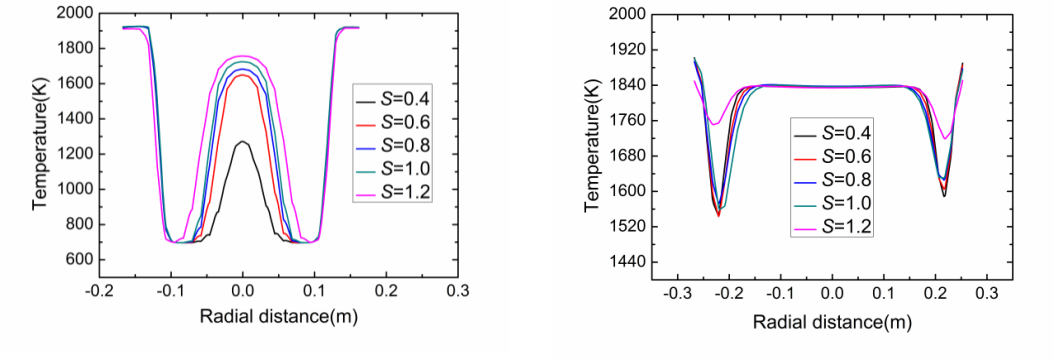

(a) x=0.98R (b) x=5.13R

Figure 9: Temperature on characteristic line at (a) x=0.98R and (b) x=5.13R under different inner swirl numbers

It can be seen from both figures that with the increase of the swirl number, the absolute value of the negative velocity in the center of the characteristic line increases gradually. However, the upper and lower boundaries of the maximum positive velocity are almost unchanged, which indicates that the range of the central recirculation zone changes little with the increase of the inner swirl number. On the characteristic line at x=0.98R, the negative velocity in the corner recirculation zone arises when the swirl number is less than 1.0. By contrast, on the characteristic line at x=5.13R, there is no negative velocity in the near-all region. The corner recirculation zone disappears at this location. This is consistent with the observation of the corner recirculation zone in last section only existed around the first boss due to the rapid evolution of the inlet swirling flow.

The temperatures on the characteristic lines at x=0.98R and x=5.13R under various inner swirl numbers are shown in Figs. 9(a)-9(b) respectively. It can be seen from Fig. 9(a) that on the line at x=0.98R, the temperature in the central recirculation zone increases with the

increase of the swirl number clearly due to the enhanced turbulent mixing of cold and hot gas caused by swirling flow. The wall temperature remains basically unchanged at about 1916.6 K. By contrast, on the characteristic line at x=5.13R, the temperature in the central recirculation zone tends to be stable as 1834 K with the varying inner swirl number. Out of this range, along the radial direction, the temperature first decreases and then increases toward the wall because the limited entrainment effect of the central recirculation flows. However, the change of the temperature along the characteristic line tends to be smooth when the swirl number increases to 1.2, due to the relatively strong mixing. The average temperature in the combustion chamber is relatively high and the average value of the exit section of the chamber is about 1831.3 K under this condition. In addition, it is noted that the temperatures around the upper and lower boundary are not strictly symmetric. It is because of the centrifugal force induced by the orientation function of inlet swirling flow.

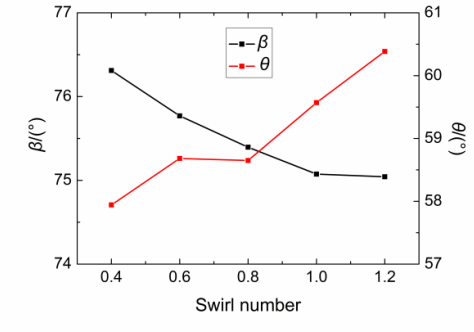

Figure 10: Volumetric average synergy angles β and θ under different swirl numbers

Fig. 10 shows the volumetric average synergy angles β and θ of the combustion chamber under different inner swirl numbers. We can see that with the increase of the swirl number, the average synergy angle β between velocity and temperature gradient decreases continuously. When the inner swirl number exceeds 1.0, the average synergy angle β is around 75.1°. This indicates that the flow field and temperature field have an excellent synergy under this condition. The heat transfer is enhanced with the increasing inner swirl number. On the other hand, we can see that the average synergy angle θ between velocity and pressure gradient increases first and then decreases, at last increases from S=0.8 with the increase of the inner swirl number. The average synergy angle θ is relatively small when the inner swirl number is between 0.4 and 0.8, which indicates that the synergy of the flow field and pressure field is excellent. In other words, the flow resistances are relatively low and the power consumptions of the heat transfer are relatively less under these conditions.

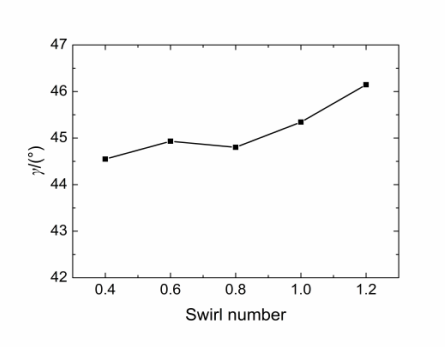

Figure 11: Volumetric average synergy angle γ under different swirl numbers

Fig. 11 shows the volumetric average synergy angle γ under different inner swirl numbers. We can see that the average synergy angle γ between velocity gradient and temperature gradient varies smoothly when the swirl number is less than 0.8. It increases gradually with the increase of inner swirl number from S=0.8. The average synergy angle γ is the largest as 46.4° when the inner swirl number is 1.2. This indicates that the velocity gradient and temperature gradient have an excellent synergy and a large comprehensive performance coefficient, which is defined as heat transfer factor over drag coefficient, according to the extended field synergy theory proposed in literature [He, Lei, Tian et al. (2009)]. Thus, the increasing inner swirl number facilitates the overall performance of heat transfer enhancement although the raise of the average synergy angle γ is limited to 2°.

3.2.2 Outer swirl number

The axial velocity on the characteristic lines at x=0.98R and x=5.13R under various swirl numbers of the inlet flow from the outer ring (outer swirl numbers) are shown in Figs. 12(a) and 12(b) respectively. The temperature on the characteristic lines at x=0.98R and x=5.13R under various outer swirl numbers are shown in Figs. 13(a) and 13(b) respectively.

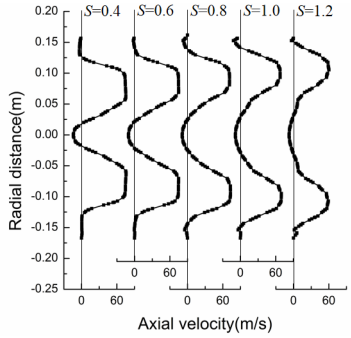

(a) x=0.98R

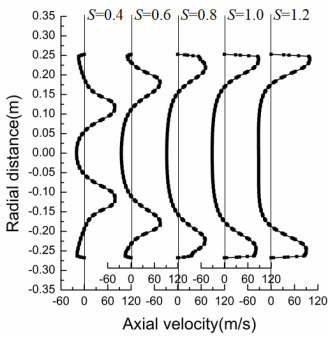

(b) x=5.13R

Figure 12: Axial velocity on characteristic line at (a) x=0.98R and (b) x=5.13R under different outer swirl numbers

It can be seen from Fig. 12(a) that with the increase of the outer swirl number, the absolute value of the negative velocity in the center of the characteristic line at x=0.98R decreases gradually. Meanwhile, the upper and lower boundaries of the maximum positive velocity move toward the wall, indicating the range of the central recirculation zone is enlarged gradually with the increase of the outer swirl number. However, on the characteristic line at x=5.13R as shown in Fig. 12(b), the absolute value of the negative velocity in the central recirculation zone increases gradually and the central recirculation zone is also enlarged as the outer swirl number increases. The corner recirculation zone generated behind the shoulder of the first boss shrinks with the increase of the outer swirl number on both lines. These influences can be explained by the fact that the increased outer swirl number makes the tangential velocity increase and the backflow caused by abrupt expansion is weakened. Thus, the boundary between the central recirculation zone and the corner recirculation zone becomes closer to the wall.

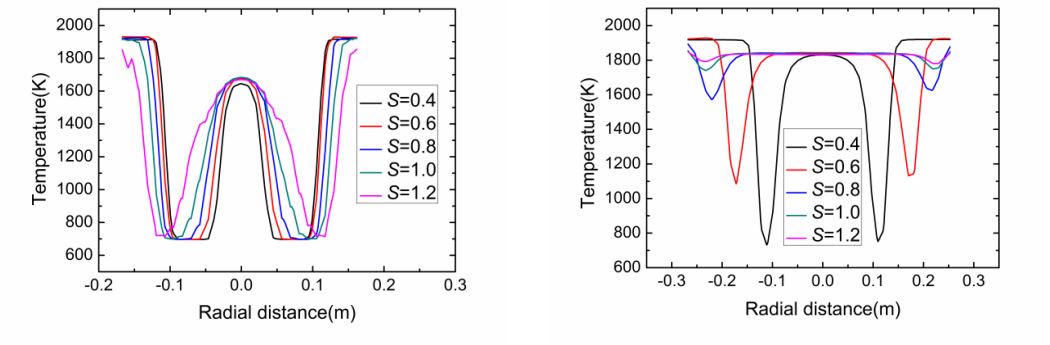

(a) x=0.98R (b) x=5.13R

Figure 13: Temperature on characteristic line at (a) x=0.98R and (b) x=5.13R under different outer swirl numbers

It can be seen from Fig. 13(a) that on the characteristic line at x=0.98R, the temperature in the section (from -0.1 m to 0.1 m of the radial distance), corresponding to the central recirculation zone, increases clearly with the increase of the swirl number because of the enhanced turbulent mixing of cold and hot gas induced by the promoted swirling strength. Moreover, the high-temperature range of the central recirculation zone is expanded with the increasing outer swirl number. The wall temperature remains unchanged at 1912 K. By contrast, on the characteristic line at x=5.13R as shown in Fig. 13(b), the range of the high-temperature central recirculation zone is also expanded with the increasing outer swirl number. The temperature at the core position tends to be stable at 1804.3 K when the outer swirl number exceeds 0.4. Moreover, the boundary of the central recirculation zone with a local minimum temperature moves toward the wall gradually. The local minimum temperature increases with the increase of the outer swirl number. It is evident that the increasing outer swirl number has a powerful impact temperature distribution in the combustion chamber. Under the condition with the outer swirl number as 1.2, the average temperature in the chamber is relatively high and the average value on the exit section is 1831.3 K.

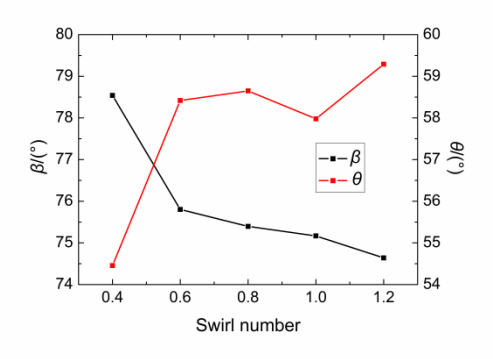

Figure 14: Volumetric average synergy angles β and θ under different outer swirl numbers

Fig. 14 shows the volumetric average synergy angles β and θ of the combustion chamber under different outer swirl numbers. According to Fig. 14, the volumetric average synergy angle β between velocity and temperature gradient is found to decrease with the increase of the outer swirl number. This indicates that with the increase of the outer swirl number, the synergy between velocity field and temperature field becomes better, and the heat transfer is enhanced. This performance is consistent with the uniform temperature distribution on the characteristic line at x=5.13R as shown in Fig. 13(b). On the other hand, the volumetric average synergy angle θ between velocity and pressure gradient is found to increase first with the increase of the outer swirl number when the swirl number is less than 0.8. The average synergy angle θ fluctuates a little under the medium swirling strength with S=0.6-1.0. However, when the outer swirl number reaches 1.2, the average synergy angle θ is relatively as large as 59.3°, which indicates that the synergy between the flow field and pressure field is relatively poor. In other words, the flow resistances are relatively large and power consumptions of the heat transfer become relatively more under these conditions than the cases with small swirl numbers.

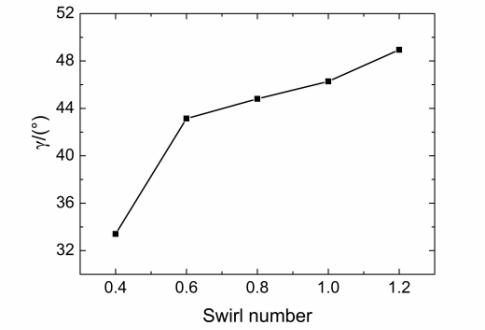

Figure 15: Volumetric average synergy angle γ under different swirl numbers

Fig. 15 shows the volumetric average synergy angle γ of the combustion chamber under different outer swirl numbers. According to Fig. 15, it is seen that the average synergy angle γ between temperature gradient and velocity gradient increases as the swirl number increases. This indicates that with the increase of the outer swirl number, the synergy

between temperature and velocity fields is getting better and the comprehensive heat transfer performance is improved. By combination of the analyses on the basis of results shown in Fig. 14, the average synergy angles γ and β have the similar effects, leading to a better heat transfer performance while the increasing θ causes a severe flow resistance in the combustion chamber. Accordingly, the synergy β plays a leading role in the overall performance of improved heat transfer under this condition.

According to the above analyses, in terms of the effects of swirl number on comprehensive thermal performance of combustion chamber, the effect of outer swirl number is larger than that of the inner swirl number. This is mainly because the mass flow rate entering the combustion chamber from the outer ring is larger than that from the inner hole. It dominates the evolution of flow, even the combustion in the chamber.

3.3 Influence of fuel-air ratio

Fig. 16 shows the axial velocity distribution along radial direction on characteristic lines at x=0.98R and x=5.13R under different fuel-air ratios of the premixed gases.

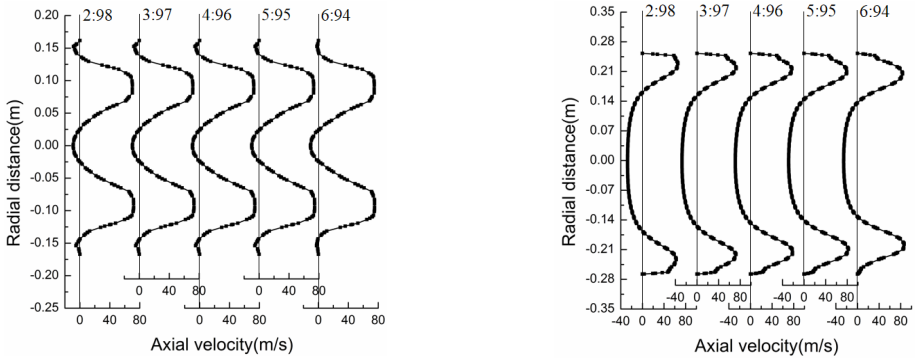

(a) x = 0.98R (b) x = 5.13R

Figure 16: Axial velocity on characteristic line at (a) x=0.98R and (b) x=5.13R under different fuel-air ratios

According to Fig. 16, on the characteristic line at x=0.98R, the fuel-air ratio has little influence on the axial velocity distribution. However, on the section x=5.13R, it is observed that with the increase of the amount of fuel in the premixed gas, the range of central recirculation zone shrinks gradually. Due to the intense chemical reaction and heat generation, the near-wall maximum axial velocity gradually increases with the increase of fuel-air ratio. When the ratio is 6:94, the average velocity at the exit of the combustion chamber is 244 m/s. It is much larger than the designed value as 170 m/s [Fu, Shi, Liu et al. (2016)].

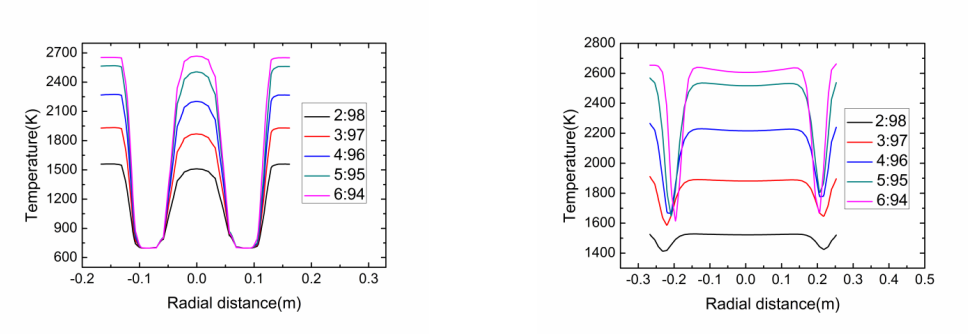

(a) x=0.98R (b) x=5.13R

Figure 17: Temperature on characteristic line at (a) x=0.98R and (b) x=5.13R under different fuel-air ratios

Fig. 17 shows temperatures on characteristic lines at x=0.98R and x=5.13R under different fuel-air ratios of the premixed gas. According to Fig. 17, the temperature in the combustion chamber generally increases with the increase of the amount of fuel in the premixed gas caused by the increase of the amount of fuel and intensity of combustion. On the characteristic line at x=0.98R, the temperature around the boundary of the central recirculation zone is stable at the inlet temperature and not affected by the fuel-air ratio owing to the non-ignition along the inlet jet flow. On the characteristic line at x=5.13R, the range of central recirculation zone shrinks gradually and the temperature gradient around the boundary increases significantly with the increase of fuel-air ratio. Moreover, when the fuel-air ratio exceeds 4:96, the temperatures in the central and corner recirculation zones of the combustion chamber both exceed 2200 K, which will lead to an increase in formation of NO_x and other pollutants. This condition cannot meet the industrial requirements for gas turbine operation.

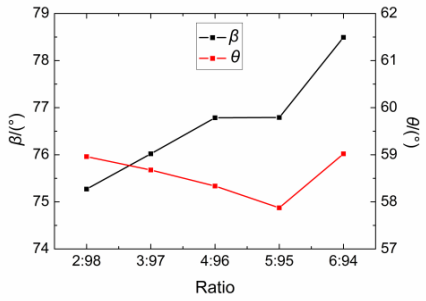

Figure 18: Volumetric average synergy angles β and θ under different fuel-air ratios

Fig. 18 shows the volumetric average synergy angles β and θ of the combustion chamber under different fuel-air ratios of the premixed gases. It is seen that the average synergy angle β between the velocity and temperature gradient increases as the amount of fuel in the premixed gas increases on the whole. However, the change of β from the ratio of 4:96 to 5:95 is very small. It means the synergy between velocity field and temperature field becomes worse and the heat transfer is weakened gradually with the increasing fuel-air

ratio. On the other hand, the average synergy angle θ between velocity and pressure gradient decreases first and then increases with the increase of the fuel-air ratio. It becomes the minimum value as 74.2° when the ratio at the inlet of the combustion chamber is 5:95. It indicates that the increase of fuel quantity can intense the synergy between velocity and pressure fields when the ratio is less than 5:95. The synergy will become poor and the flow resistance increases after fuel-air ratio exceeds 5:95 for the present combustion chamber.

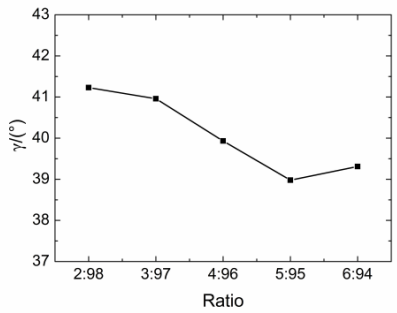

Figure 19: Volumetric average synergy angle γ under different fuel-air ratios

Fig. 19 shows the volumetric average synergy angle γ under different fuel-air ratios of the premixed gases. It is seen that when the amount of fuel in the premixed gas increases, the average synergy angle γ between the velocity gradient and temperature gradient decreases until the ratio of 5:95. It indicates that the synergy between the velocity and temperature fields becomes bad and the overall performance of low-resistance heat transfer in combustion chamber becomes worse with the increasing fuel-air ratio. This is induced by the enhanced combustion caused by more fuel entered, which results in a large and rapid temperature raise in the chamber. Thus, its expansion causes relatively large flow resistance although the heat transfer is enhanced.

3.4 Influence of inlet gas temperature

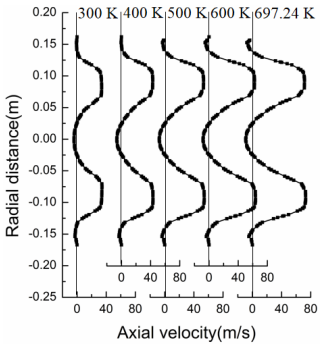

(a) x=0.98R

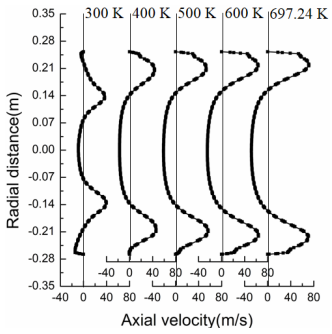

(b) x=5.13R

Figure 20: Axial velocity on characteristic line at (a) x=0.98R and (b) x=5.13R under different inlet gas temperatures

The axial velocities on the characteristic lines at x=0.98R and x=5.13R under various temperatures of the inlet premixed gas are shown in Figs. 20(a) and 20(b) respectively. It can be seen that with the increase of inlet temperature, the absolute value of the negative velocity in the center of the central recirculation zone gradually increases, while that in the corner recirculation zone gradually decreases on both lines. Meanwhile, out of the central recirculation zone, the local maximum positive velocity increases as the inlet temperature increases. On the characteristic line at x=0.98R, the axial velocity gradient in the central recirculation zone increases with the increase of inlet temperature. However, it tends to be equivalent with the increasing inlet temperature on the line at x=5.13R due to the evolution of the gas flow.

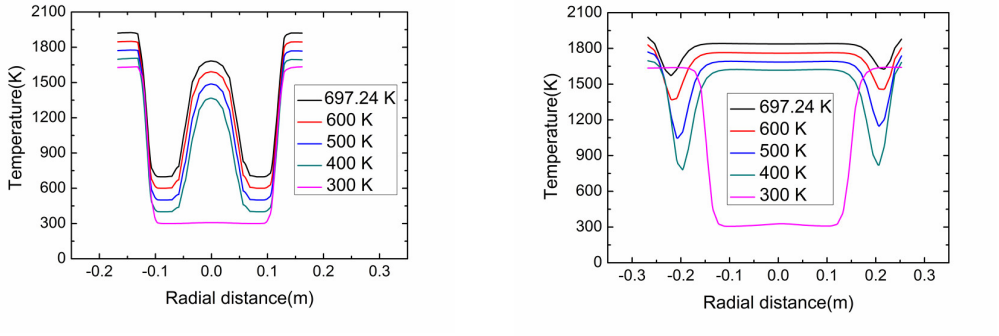

(a) x=0.98R (b) x=5.13R

Figure 21: Temperature on characteristic line at (a) x=0.98R and (b) x=5.13R under different inlet gas temperatures

The temperatures on the characteristic lines at x=0.98R and x=5.13R under various inlet gas temperatures are shown in Figs. 21(a) and 21(b) respectively. It can be seen from Fig. 21(a) that on the line at x=0.98R, the temperature in the central recirculation zone and the near-wall region increases with the increase of the inlet gas temperature clearly due to the intensive combustion caused by hot premixed gas. However, the high-temperature range of the central recirculation zone is stable. By contrast, on the characteristic line at x=5.13R, the range of the high-temperature central recirculation zone is expanded with the increase of inlet temperature. The temperature at the core position increases to 1804.3 K when the inlet temperature increases to the designed value as shown in Fig. 21(b). Moreover, the boundary of the central recirculation zone with a local minimum temperature moves toward the wall gradually. The local minimum temperature increases with the increase of the inlet temperature.

By the comparison between Figs. 21(a) and 21(b), on the downstream line at x=5.13R, the high-temperature central recirculation zone is expanded due to the evolution of the combustion and gas flow. More results show that with the decrease of the inlet premixed gas temperature, the average temperature of the outlet section of the combustion chamber decreases by a multiple of 0.92-0.96. It is noted that when the inlet gas temperature is 300 K, the temperature in the central recirculation zone on both lines is basically 300 K, indicating that the combustion has not started and a heating process is required for the gas combustion. Further investigation shows that the reaction process along the chamber axis

is started at the location close to the exit of the combustion chamber. The average temperature at the exit of chamber is the lowest as 1455 K among all the investigated cases when the inlet temperature of premixed gas is 300 K.

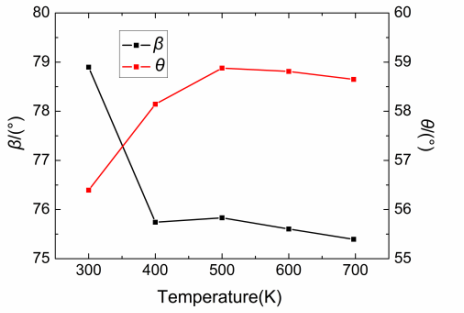

Figure 22: Volumetric average synergy angles β and θ under different inlet gas temperatures

Fig. 22 shows the volumetric average synergy angle β and θ of the combustion chamber under different inlet temperatures. It is found that the average synergy angle β between velocity and temperature gradient decreases abruptly with the increase of the inlet temperature from 300 K to 400 K. The decrease of the synergy angle is slight when the temperature exceeds 400 K. This indicates that the inlet gas temperature of 300 K is not desirable. The synergy between the velocity field and the temperature field becomes better, and the heat transfer is enhanced with the increasing temperature. On the other hand, the volumetric average synergy angle θ between velocity and pressure gradient increases with the increase of the inlet temperature when it is less than 500 K. The synergy angle θ tends to decline slowly when it exceeds 500 K. This indicates that the synergy of the flow field and pressure field becomes poor when the inlet temperature is over 400 K. In other words, the flow resistances are relatively large and power consumptions of the heat transfer increase when the inlet temperature exceeds a certain value.

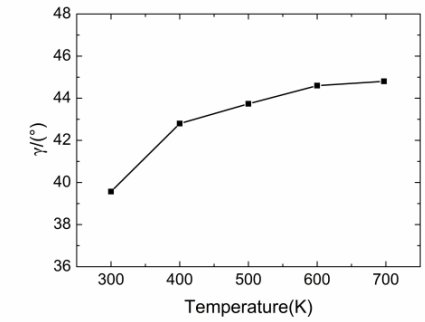

Figure 23: Volumetric average synergy angle γ under different inlet gas temperatures

Fig. 23 shows the volumetric average synergy angle γ under different inlet gas temperatures. From Fig. 23, it is seen that the average synergy angle γ increases with the increase of the inlet temperature. This also means that as the inlet temperature increases, the synergy

between temperature and velocity fields is getting better and the comprehensive heat transfer performance is enhanced accordingly. By combination of the analyses on the basis of results shown in Fig. 22, the average synergy angles γ and β have the similar effects to make a better heat transfer performance while the increasing θ results in a severe flow resistance in the combustion chamber. Accordingly, the synergy β is evident to play a leading role in the overall performance of enhanced heat transfer under this condition.

4 Conclusions

In this study, the combustion coupled with gas flow, heat transfer process in a large-size annular combustion chamber is investigated numerically for a heavy-duty gas turbine. The influences of the swirl number of the double-swirler inlet flow, the fuel-air ratio and temperature of the premixed gas on the multi-field synergy among the velocity, temperature and pressure fields are studied. The conclusions are drawn as follows:

(1) The outer swirl number has greater influences on the multi fields and their synergy in the combustion chamber than the inner swirl number. The central recirculation zone formed in the chamber is developed and expanded with the increase of swirl number and temperature and the decrease of fuel-air ratio. The excellent multi-field synergy of the central recirculation zone leads to the uniform temperature distribution on the downstream characteristic lines with the evolution of swirling flow.

(2) With the increase of swirl number and gas temperature of inlet flow, the entire volumetric average synergy angle β between the velocity and temperature gradient decreases. Meanwhile, the synergy angle θ between the velocity and pressure gradient and the synergy angle γ between the velocity gradient and temperature gradient increases. The increasing fuel-air ratio of the premixed gas has reverse effects on the synergy angles. The designed condition of the combustion chamber with double swirl numbers as 0.8, inlet temperature as 697.24 K and fuel-air ratio as 2:98 can obtain a relatively excellent multi-field synergy.

(3) The heat transfer in the combustion chamber is enhanced as indicated and the flow resistance and power consumption are raised with the increasing inlet swirl number and gas temperature, and the decreasing fuel-air ratio of premixed gas. Meanwhile, the comprehensive performance of low-resistance heat transfer is achieved. The synergy angle β plays a leading role for the comprehensive performance of low-resistance heat transfer with the varying factors.

Acknowledgement: The supports by the National Natural Science Foundation of China (No.51606114) and Science and Technology Commission of Shanghai Municipality (Nos.19020500900, 16020500700) to this study are acknowledged and highly appreciated.

Conflicts of Interest: The authors declare that they have no conflicts of interest to report regarding the present study.

References

Aklouche, F. Z.; Loubar, K.; Bentebbiche, A.; Awad, S.; Tazerout, M. (2017): Experimental investigation of the equivalence ratio influence on combustion, performance and exhaust emissions of a dual fuel diesel engine operating on synthetic biogas fuel. *Energy Conversion and Management*, vol. 152, no. 52, pp. 291-299.

Anacleto, P. M.; Fernandes, E. C.; Heitor, M. V.; Shtork, S. I. (2003): Swirl flow structure and flame characteristics in a model lean premixed combustor. *Combustion Science and Technology*, vol. 175, no. 8, pp. 1369-1388.

Ayodele, B. E.; Vincent, E.; Claudius, A.; Lanre, O.; Dickson, E. (2019): Data-based investigation on the performance of an independent gas turbine for electricity generation using real power measurements and other closely related parameters. *Data in Brief*, vol. 26, pp. 1-16.

Chen, F.; Ruan, C.; Yu, T.; Cai, W.; Mao, Y. et al. (2019): Effects of fuel variation and inlet air temperature on combustion stability in a gas turbine model combustor. *Aerospace Science and Technology*, vol. 92, pp. 126-138.

Dang, X. X. (2009): *Experimental Investigation and Numerical Simulation of a Gas Turbine Annular Combustor with Dual-Stage Swirler*. Doctoral dissertation, Nanjing University of Aeronautics and Astronautics, Nanjing, China (In Chinese).

E, J. Q.; Liu, H. J.; Zhao, X. H.; Han, D. D.; Peng, Q. G. et al. (2018): Investigation on the combustion performance enhancement of the premixed methane/air in a two-step micro combustor. *Applied Thermal Engineering*, vol. 141, pp. 114-125.

Fu, Z. G.; Shi, L.; Liu, B. H.; Shen, Y. Z. (2016): Numerical simulation of NOx formation in a heavy duty gas turbine annular combustion chamber. *Journal of Engineering for Thermal Energy and Power*, vol. 31, no. 4, pp. 52-58 (In Chinese).

Gao, H. H.; Fu, Z. G.; Zeng, Z. X.; Liu, J.; Weng, P. F. (2019): Effects of swirling strength of the premixed gas flow on pollutant emission in a heavy-duty gas turbine. *E3S Web of Conferences*, vol. 118, 04038.

Guo, Z. Y.; Li, D. Y.; Wang, B. X. (1998): A novel concept for convective heat transfer enhancement. *International Journal of Heat and Mass Transfer*, vol. 41, no. 14, pp. 2221-2225.

Guo, Z. Y.; Tao, W. Q.; Shah, R. K. (2005): The field synergy (coordination) principle and its applications in enhancing single phase convective heat transfer. *International Journal of Heat and Mass Transfer*, vol. 48, no. 9, pp. 1797-1807.

Han, X.; Laera, D.; Morgans, A. S.; Lin, Y. Z.; Zhang, C. et al. (2019): Inlet temperature driven supercritical bifurcation of combustion instabilities in a Lean Premixed Prevaporized combustor. *Experimental Thermal and Fluid Science*, vol. 109, pp. 1-11.

He, Y. L.; Lei, Y. G.; Tian, L. T.; Chu, P.; Liu, Z. B. (2009): Analysis of three-field synergy on heat transfer augmentation with low penalty of pressure drop. *Journal of Engineering Thermophysics*, vol. 30, no. 11, pp. 1904-1906. (In Chinese)

Huang, Y.; Yang, V. (2004): Bifurcation of flame structure in a lean-premixed swirl-stabilized combustor: transition from stable to unstable flame. *Combustion and Flame*, vol. 136, no. 3, pp. 383-389.

Jin, G.; Zhang, Z. X.; Gu, M. Q. (2008): Numerical simulation of QD128 aero-derivative gas turbine combustor. *Aeroengine*, vol. 34, no. 2, pp. 34-39 (in Chinese).

Karim, V. M.; Bart, M. (2006): Application of two buoyancy-modified k-ε turbulence models to different types of buoyant plumes. *Fire Safety Journal*, vol. 41, no. 2, pp. 122-138.

Lee, J. H.; Kim, T. S.; Kim, E. (2017): Prediction of power generation capacity of a gas turbine combined cycle cogeneration plant. *Energy*, vol. 124, pp. 187-197.

Li, G.; Jiang, X.; Zhu, J.; Yang, J.; Liu, C. et al. (2019): Combustion control using a lobed swirl injector and a plasma swirler. *Applied Thermal Engineering*, vol. 152, pp. 92-102.

Liu, H. L.; Li, H.; He, Y. L.; Chen, Z. T. (2018): Heat transfer and flow characteristics in a circular tube fitted with rectangular winglet vortex generators. *International Journal of Heat and Mass Transfer*, vol. 126, pp. 789-1006.

Liu, W.; Liu, P.; Wang, J. B.; Zheng, N. B.; Liu, Z. C. (2018): Exergy destruction minimization: a principle to convective heat transfer enhancement. *International Journal of Heat and Mass Transfer*, vol. 122, pp. 11-21.

Liu, W.; Liu, P.; Dong, Z. M.; Yang, K.; Liu, Z. C. (2019): A study on the multi-field synergy principle of convective heat and mass transfer enhancement. *International Journal of Heat and Mass Transfer*, vol. 134, pp. 722-734.

Liu, W.; Liu, Z. C.; Huang, S. Y. (2010): Physical quantity synergy in the field of turbulent heat transfer and its analysis for heat transfer enhancement. *International Journal of Heat and Mass Transfer*, vol. 55, no. 23, pp. 2589-2597.

Lu, G. F.; Zhou, G. B. (2016): Numerical simulation on performances of plane and curved winglet pair vortex generators in a rectangular channel and field synergy analysis. *International Journal of Thermal Sciences*, vol. 109, pp. 323-333.

Mohammad, B.; Jeng, S. M.; Andac, M. G. (2010): Influence of the primary jets and fuel injection on the aerodynamics of a prototype annular gas turbine combustor sector. *ASME Turbo Expo 2010: Power for Land, Sea, and Air.*

Nam, J.; Lee, Y.; Joo, S.; Yoon, Y.; Yoh, J. J. (2019): Numerical analysis of the effect of the hydrogen composition on a partially premixed gas turbine combustor. *International Journal of Hydrogen Energy*, vol. 44, no. 12, pp. 6278-6286.

Orbay, R. C.; Nogenmyr, K. J.; Klingmann, J.; Bai, X. S. (2013): Swirling turbulent flows in a combustion chamber with and without heat release. *Fuel*, vol. 104, pp. 133-146.

Palm, R.; Grundmann, S.; Weismüller, M.; Tropea, C. (2006): Experimental characterization and modelling of inflow conditions for a gas turbine swirl combustor. *International Journal of Heat and Fluid Flow*, vol. 27, no. 5, pp. 924-936.

Tang, L. H.; Chu, W. X.; Ahmed, N.; Zeng, M. (2016): A new configuration of winglet longitudinal vortex generator to enhance heat transfer in a rectangular channel. *Applied Thermal Engineering*, vol. 104, pp. 74-84.

Tao, W. Q.; Guo, Z. Y.; Wang, B. (2002): Field synergy principle for enhancing convective heat transfer-its extension and numerical verifications. *International Journal of Heat and Mass Transfer*, vol. 45, no. 18, pp. 3849-3856.

Tao, W. Q.; He, Y. L.; Wang, Q. W.; Qu, Z. G.; Song, F. (2002): A unified analysis on enhancing single phase convective heat transfer with field synergy principle. *International Journal of Heat and Mass Transfer*, vol. 45, pp. 4871-4879.

Tsao, J. M.; Lin, C. A. (1999): Reynolds stress modelling of jet and swirl interaction inside a gas turbine combustor. *International Journal for Numerical Methods in Fluids*, vol. 29, no. 4, pp. 451-464.

Vishwanath, R. B.; Tilak, P. M.; Chaudhuri, S. (2018): An experimental study of interacting swirl flows in a model gas turbine combustor. *Experiments in Fluids*, vol. 59, no. 3, pp. 1-17.

Worth, N. A.; Dawson, J. R. (2017): Effect of equivalence ratio on the modal dynamics of azimuthal combustion instabilities. *Proceedings of the Combustion Institute*, vol. 36, no. 3, pp. 3743-3751.

Xie, X. C.; He, C.; Zhang, B.; Chen, Q. (2018): Heat transfer enhancement for the coil zone of closed wet cooling towers through field synergy analysis. *Computer Aided Chemical Engineering*, vol. 44, pp. 1927-1932.

Zeng, Z. X.; Wang, Z. K.; Tian, J. Y.; Xu, Y. H. (2015): Numerical analysis of multi-field synergy in advanced vortex combustor. *Journal of Propulsion Technology*, vol. 36, no. 12, pp. 1859-1867.

Zhang, C. C.; Wang, D. B.; Zhu, Y. J.; Han, Y.; Wu, J. X. et al. (2015): Numerical study on heat transfer and flow characteristics of a tube fitted with double spiral spring. *International Journal of Thermal Sciences*, vol. 94, pp. 18-27 (In Chinese).

Zhang, Z. B.; Zheng, H. T.; Zhao, Y. (2013): Effects of turbulence combustion models on performance of the gas turbine combustor. *Gas Turbine Technology*, vol. 26, no. 4, pp. 22-27 (In Chinese).